

A new SDOF method of one-way reinforced concrete slab under non-uniform blast loading

Wei Wang^{*1,2}, Duo Zhang², Fangyun Lu² and Ruichao Liu¹

¹Luoyang Institute of Hydraulic Engineering and Technology, Luoyang 470123, Henan, China

²Institute of Technique Physics, College of Science, National University of Defense Technology, Changsha, Hunan 410073, P.R. China

(Received November 1, 2012, Revised March 31, 2013, Accepted April 24, 2013)

Abstract. A new effective model for calculation of the equivalent uniform blast load for non-uniform blast load such as close-in explosion of a one-way square and rectangle reinforced concrete slab is proposed in this paper. The model is then validated using single degree of freedom (SDOF) system with the experiments and blast tests for square slabs and rectangle slabs. Test results showed that the model is accurate in predicting the damage level on the tested RC slabs under the given explosive charge weight and stand-off distance especially for close-in blast load. The results are also compared with those obtained by conventional SDOF analysis and finite element (FE) analysis using solid elements. It is shown that the new model is more accurate than the conventional SDOF analysis and is running faster than the FE analysis.

Keywords: blast load; equivalent load; SDOF; one-way reinforced concrete slab

1. Introduction

In recent years, explosive incidents due to terrorist attack and accidental explosion have increased in the world (Luccioni *et al.* 2004, Osteraas 2006, Islama and Yazdani 2008). The behavior analysis and design of hardened structures for protection against short duration dynamic loading, such as those induced by air blast, is a subject of extensive studies in the last decades. It has been recognized that the intensive dynamic loading by detonations should be taken into account in the structural design for both military and civilian structures and facilities in such cases.

As reinforced concrete slabs are the main members of a structure, the analysis of reinforced concrete slab under blast loading has been conducted for a long time in recent years. For example, Silva and Lu (2007, 2009) studied a procedure to estimate how the explosive charge weight and stand-off distance impose certain levels of damage on reinforced concrete RC slabs. Ohkubo *et al.* (2008) and Wu *et al.* (2009) evaluated the effectiveness of fiber sheet reinforcement on the explosive-resistant performance of concrete plates. Wang *et al.* (2012b, 2013b) addressed the scaling of the dynamic response of one-way square reinforced concrete slabs subjected to close-in blast loadings. Advanced numerical methods such as mesh free methods and finite element methods in recent years have been developed to simulate of reinforced concrete structures

*Corresponding author, Ph.D., E-mail: wangwei591@126.com

subjected to air blast loads (Nash *et al.* 1995, Rabczuk and Eibl 2003, Rabczuk *et al.* 2004, Zhou *et al.* 2005, Xu and Lu 2006). However, few studies have been carried out to estimate the damage modes and damage mechanism of one-way square reinforced concrete slabs subjected to close-in blast loading.

Reinforced concrete slabs are typically analyzed for blast loadings using one of two methods of very different complexity: (1) equivalent single degree of freedom (SDOF) analysis (Biggs 1964, Mays and Smith 1995, Wang *et al.* 2012a); and (2) finite element analysis methods (Rabczuk and Eibl 2003, Rabczuk *et al.* 2004, Zhou *et al.* 2005, Xu and Lu 2006). SDOF methods are common nowadays for blast design of protective structural elements (Mays and Smith 1995, Krauthammer 1999, Bangash and Bangash 2006, Wang *et al.* 2013a). This is the case even as many other powerful finite element methods have been developed in the last decades. The SDOF model is widely used in design because it presents several advantages such as ease of use and low running time, which have made it appealing for blast design and incorporation into design manuals (TM5-1300 1990, PDC-TR-06-01(Rev1) 2008, UFC-3-340-02 2008) for the blast analysis and design of building components. However, conventional SDOF analysis is incapable of capturing a spatially and temporally varying distribution of blast loading, cannot allow for variations of mechanical properties of the cross-section along the member, cannot simultaneously accommodate shear and flexural deformations, can only address strain rate effects indirectly, and can produce very conservative answers. A finite element analysis using codes such as LS-DYNA (LS-DYNA 2007) and AUTODYN (AUTODYN 2006) can be applied to analyze the structural response to blast loads (Luccioni *et al.* 2004) but such an analysis is rarely used because of its perceived complexity and time consuming.

In this paper, a new effective SDOF method for calculation of the equivalent uniform blast load for non-uniform blast load is described herein. The proposed method captures key attributes of the non-uniform loading on the square reinforced concrete slab but retains much of the simplicity associated with equivalent SDOF analysis. The accuracy of the proposed method is validated using data from field blast testing of square slabs and rectangle slabs. This paper presents key analytical and experimental results that can substantiate this main conclusion. At last, the results of the SDOF analysis are then compared with those from both a conventional SDOF analysis and a detailed finite element analysis.

2. Conventional SDOF method under blast loading

The SDOF system for modeling the flexural response is based on Biggs (1964), where the deflected shape of the structure is assumed to be the same as that resulting from the static application of the dynamic load. This is illustrated in Fig. 1. The equivalent mass and stiffness parameters are derived based on the mass density, Young's modulus, moment inertia, span length and boundary condition of the slab, as well as the deflection shape of the slab under uniform distributed static load. More details can be found in Biggs (1964). The simplification for flexural response has been widely accepted and recommended in Protective design manuals (TM5-1300 1990; PDC-TR-06-01(Rev1) 2008, UFC-3-340-02 2008). With effective factors, such SDOF system can give out maximum displacement, velocity and acceleration quickly. Consequently damage assessment can be carried out based on the maximum displacement of the structure or elements.

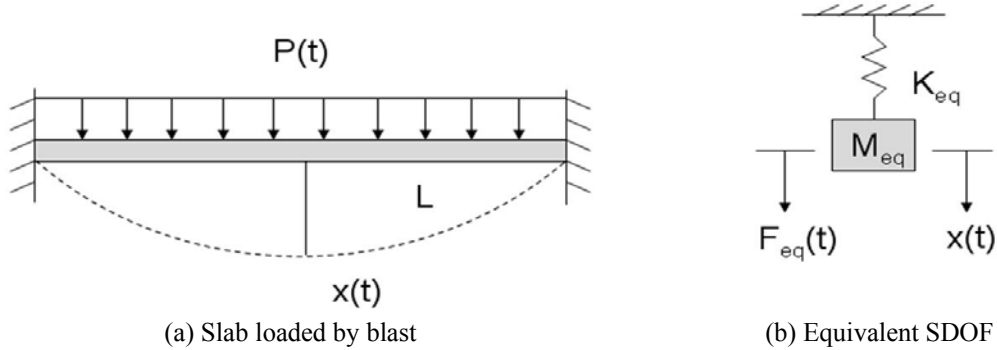


Fig. 1 Equivalent spring-mass SDOF system

Upon transforming the structural slab into its equivalent flexural SDOF system, the governing differential equation of a beam without damping is presented as follows (TM5-1300 1990)

$$K_M M \ddot{x}(t) + K_L R(x) = K_L F_c(t) \tag{1}$$

or

$$K_{LM} M \ddot{x}(t) + R(x) = F_c(t) \tag{2}$$

$$K_{LM} = \frac{K_M}{K_L} \tag{3}$$

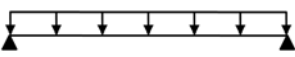
where x is the midspan deflection, M is the total mass of beam, $R(x)$ is resistance of beam, $F_c(t)$ is applied force, K_M is mass factor of beam, K_L is load factor of beam, and K_{LM} is load-mass factor of beam. K_M and K_L are determined to have the same energy distribution as that of the continuous beam responding in an assumed mode shape and can be computed as Eq. (3).

$$K_L = \frac{\int_0^L p(x)\varphi(x)dx}{\int_0^L p(x)dx} \tag{4}$$

$$K_M = \frac{\int_0^L m(x)\varphi^2(x)dx}{\int_0^L m(x)dx} \tag{5}$$

where $p(x)$ is the dynamic load on blast-loaded component, $\varphi(x)$ is the deflected shape function of the blast-loaded component, $m(x)$ is mass per unit length of the blast-loaded component. Based on the assumed deflected shape K_M and K_L are shown in Table 1 (TM5-1300 1990). Fig. 2 shows an

Table 1 Load, mass, and load-mass factors

Boundary Condition and Loading Diagram	Range of Behavior	Load Factor K_L	Mass Factor K_M	Load-Mass Factors K_{LM}
	Elastic	0.64	0.50	0.78
	Plastic	0.50	0.33	0.66

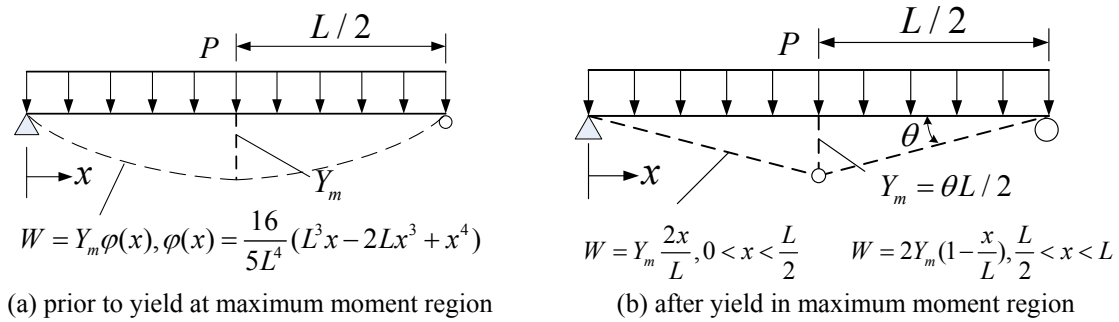


Fig. 2 Deflected Shape Functions for Simply Supported Beam

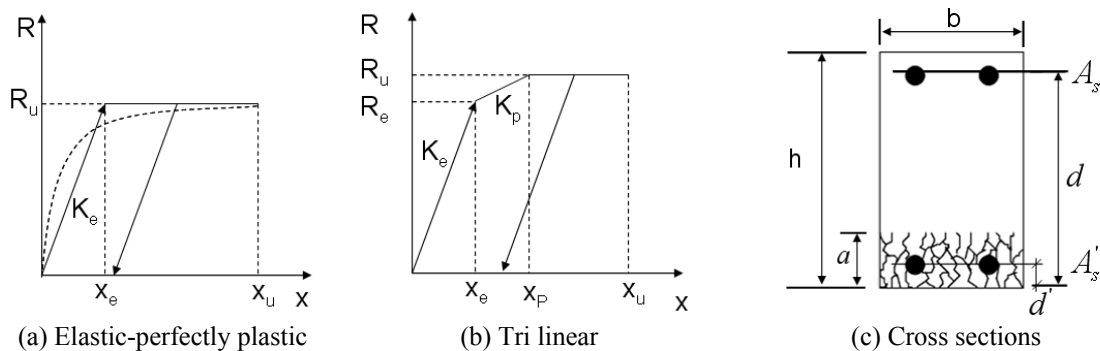


Fig. 3 Nonlinear resistance functions and their idealization of beam

example of assumed assumed deflected shape functions, $\varphi(x)$, for a one-way component (i.e., a beam) with a uniformly distributed load and simple supports during elastic response and during plastic response, which occurs after the component has yielded at all maximum moment regions and becomes a mechanism.

The resistance function ($R-x$) of concrete structures under blast load is highly nonlinear. In this paper the function of structures is assumed to be elastic-perfectly plastic for simple support beam and tri-linear resistance functions for fixed support beam respectively and the slope of the unloading path is the same as that of loading path, as shown in Fig. 3 (a) and (b).

The stiffness in the elastic domain and ultimate resistance which would cause a simple support beam yielding are shown as followings (TM5-1300 1990)

$$K_e = \frac{384EI_e}{5L^3} \tag{6}$$

$$R_u = \frac{8M_u}{L} \tag{7}$$

where K_e is stiffness of the beam in elastic domain of beam resistance function, L is the length of the beam, E is the elastic modulus of the concrete, I_e is the inertia moment of the beam, R_u is ultimate resistance and M_u is the ultimate theoretical plastic moment capacity. In this paper M_u is computed as following (Krauthammer 2008)

$$M_u = A_s f_{dy} (d - d') + (A_s - A'_s) f_{dy} (d - a / 2) \tag{8}$$

in which

$$a = [(A_s - A'_s) f_{dy}] / 0.85 f'_c b \tag{9}$$

where a equals to depth of the concrete compression block, A_s and A'_s represent tensile and compressive reinforcement areas, respectively. b is the beam width, h is the total thickness/depth, d' is the distance from top compression face to center of the compression steel, d is the effective depth (distance from top fiber to center of tensile reinforcement), f_{dy} is the steel yield stress, f'_c is the concrete uniaxial strength. All above are shown in Fig. 3(c). It is assumed for the ultimate state that one can use a rectangular stress block for concrete in compression, elasto-plastic steel, and concrete in tension is ignored. These types of relationships also apply to one-way slabs.

A numerical integration method can be used to solve for the displacement-time history of a single-degree-of-freedom system (Tedesco *et al.* 1999). In this paper the Newmark-Beta method was adopted to solve the SDOF model numerically (Newmark 1962). The Newmark-Beta method is most commonly used in available computer programs that solve the SDOF equation of motion in this manner. The constant velocity method is probably the simplest numerical method recommended for solving the equation of motion for blast design and analysis problems (Biggs 1964). The US Army uses the minimum value between 10% of the natural period and 3% of triangle positive loading duration as time step to solve an inelastic SDOF model (PDC-TR-06-01(Rev1) 2008). In this study, the time step was 0.1% of smallest value of natural periods and positive loading duration, which is compared to US Army approach.

The following steps are performed when the SDOF model is the main analysis tool used to assess a structural component under airblast loading (PDC-TR-06-01(Rev1) 2008):

- (1) The maximum allowable ductility ratio and support rotation are determined by protection level for the component types.
- (2) The airblast load is estimated considering the charge weight, standoff distance, and the angle between the explosion point and the normal plane of the member.
- (3) The maximum ductility ratio which is defined in Equation (10) and support rotation which is defined in Fig. 2(b) of the member are calculated by using the SDOF method.

$$\mu = \frac{y_m}{y_e} \tag{10}$$

in which y_m is maximum component deflection and y_e is deflection causing yield of the member.

- (4). The calculated maximum ductility ratio and support rotation are compared to the predetermined maximum allowable ductility ratio and support rotation for a user defined building level of protection (LOP) from the DoD and a user defined component framing type (i.e.,

secondary or primary component).

(5). If the calculated response satisfies the allowable response, the member is safe. If not, the member is damaged.

3. Equivalent uniform blast load

As shown in (PDC-TR-06-01(Rev1) 2008), it can be very difficult to model component response to blast loads with complex spatial load distributions using a conventional SDOF analysis. Blast loads that vary significantly over the area of a structural component, such as close-in explosions, must be converted into an “equivalent” blast load that is spatially uniform over the whole area of the component at each time step because the load factor in SDOF analyses almost always assumes spatially uniform loading.

In this section an “equivalent” blast load is computed based on equating the external virtual work done by the equivalent uniform blast load to the external virtual work done by the non-uniform blast load such as close-in explosions.

3.1 Blast load histories

The blast loading in the SDOF system is applied on the member as a function of space and time. This allows an arbitrary load distribution to be applied to the member. The shape of the distributed load across the member is dependant on the charge weight, shape and standoff distance and the pressure history can be predicted by current code such as TM5-1300 (1990) or using the measured pressure history directly.

In this paper, the blast load history on the slabs of different point is assumed to be with the same duration but not with the same peak pressure as shown Fig. 4. It is accepted and recommended by Jones (2009) and Wu *et al.* (2009) from experimental pressure readings. The experimental pressure readings demonstrate that the pentagonal distributed load as shown in Fig. 4(a) is a better approximation of the actual blast load; an expected result given that the standoff distance and angle of incidence change as a function of location on the slab. Variables $P_{r_{maxC}}$ and $P_{r_{max}}$ are the peak pressures at the center and the edge, respectively. Although the arrival time at the center is earlier than at the supports, the definite lag is very small as compared with the response of the slab. For simplicity we choose to ignore the lag in this paper. The pressure time histories at the center and edge are simplified as triangular blast loads as shown in Fig. 4(b). The duration of the positive pressure wave t_d was back-calculated as

$$t_d = \frac{2i_r}{P_{r_{max}}} \quad (11)$$

where i_r is the measured positive impulse at the center and the edge. For analysis, the reported values of the peak load were assumed to apply over the full width of the slab. Since negative phase may uplift of the slab panel but the difference is very mirror, by the same time the negative pressure phase does not affect significantly the maximum transient displacement of the panel and should have only a small effect on the residual displacement as shown in Jones *et al.* (2009) and Wu *et al.* (2009), we chose to ignore the negative phase for our computations.

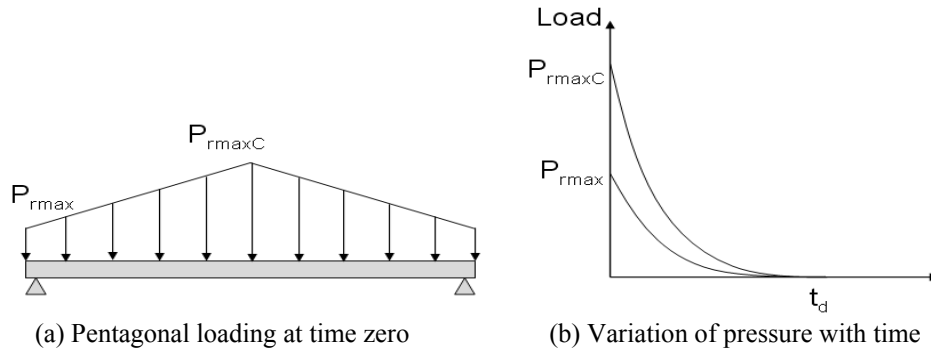


Fig. 4 Simplified pressure distributions

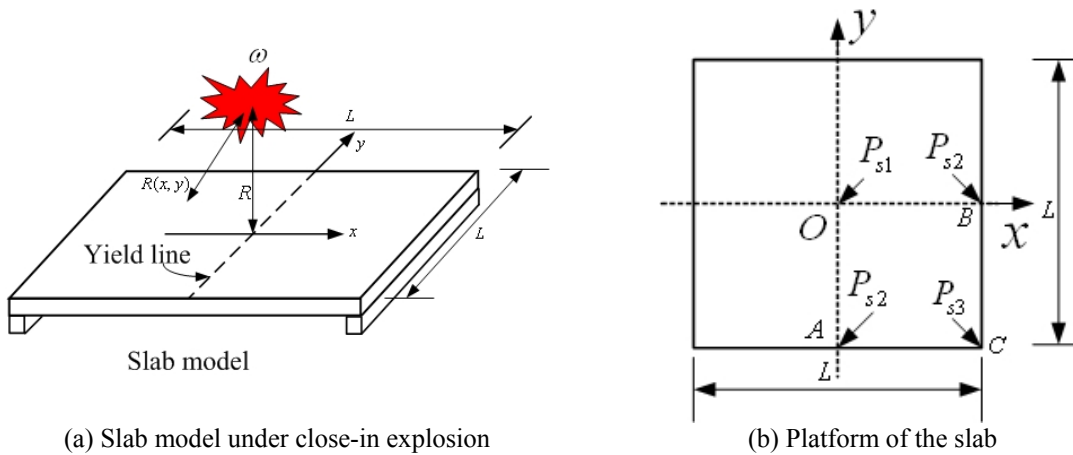


Fig. 5 Failure model of a simply supported square reinforced concrete slab

3.2 Equivalent analysis

Although Silva and Lu (2007, 2009) studied a procedure to convert dynamic point loads into uniform blast pressure, they did not consider the transformation of the non-uniform distributed blast load into uniform blast pressure. In this paper, the transformation of the non-uniform distributed blast load into uniform blast pressure is studied for SDOF analysis by the same external virtual work done.

A simply supported square reinforced concrete slab is model here to study the equivalent load shown in Fig. 5. A typical peak pressure $P(x, y)$ distribution on a square slab is shown in Fig. 6. From Fig. 6, one can find that the blast pressure on the reinforced concrete slab is non-uniform for a close-in explosion. The pressure wave is significantly higher at the center of the slabs and dissipates rapidly towards the ends of the slab shown in Fig. 6. The peak pressure of the center O is noted as P_{s1} , the peak pressure of the edge A and B is noted as P_{s2} , and the peak pressure of the corner C is noted as P_{s3} which is shown in Fig. 5(b).

In this paper, the ratio of slab width to thickness is supposed to be larger than 10, and the failure model of the square slab is on the assumption of flexural failure in center yield line for the

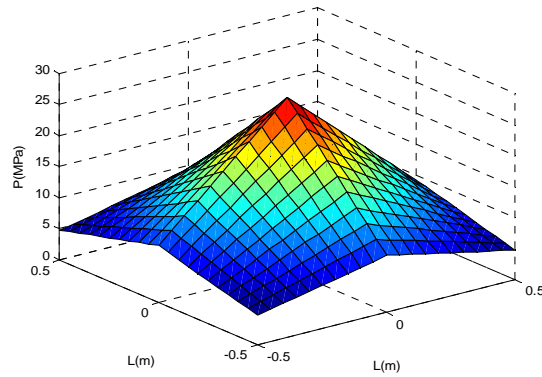
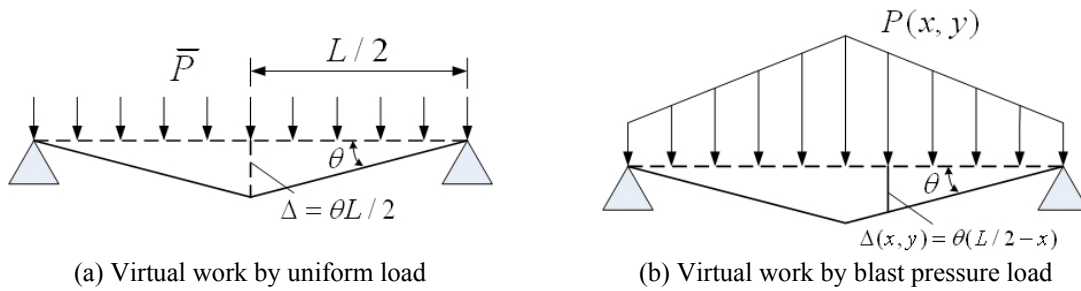


Fig. 6 A typical three-dimensional peak pressure distribution of the square RC slab



(a) Virtual work by uniform load
 (b) Virtual work by blast pressure load
 Fig. 7 Failure mechanism of a simply supported square reinforced concrete slab

blast load and plastic hinges with zero length. The equivalent uniform blast load is shown in Fig. 7. In real tests, the hinges have a finite length. If we considered the effect of a finite length hinges, the length of the slab should be subtracted with the hinges length.

The response limits for the boundaries of component damage levels for reinforced concrete members are shown in (PDC-TR-06-01(Rev1) 2008). It is found that the biggest support rotation θ for serious damage level boundary is 10 degree. It is small enough that the deformation of the slab can be on the assumptions of linearly elastic, small deformation response before it is damaged by the blast load.

Assuming symmetric load and deflection distributions for small deformation response, the support rotation θ is defined by the ratio of the calculated peak deflection to half a span length for one-way slabs

$$\tan \theta = \frac{2\Delta}{L} \tag{12}$$

Where L is span length of the element, and Δ is the max displacement of the center. Since θ is small enough, $\tan \theta$ approximately equals to θ . Then Δ can be expressed as

$$\Delta = \frac{\theta L}{2} \tag{13}$$

The peak pressure function $P(x, y)$ is the assumed shape of the blast pressure wave and is developed by using the blast pressure waves presented in Fig. 4. In this paper, $P(x, y)$ can be simply expressed as

$$P(x, y) = P_{s1} + \frac{2}{L}(P_{s2} - P_{s1})(x + y) + \frac{4}{L^2}xy(P_{s3} + P_{s1} - 2P_{s2}), \tag{14}$$

$$0 \leq x, y \leq L/2$$

where P_{s1} , P_{s2} and P_{s3} are either by using the measured reflected pressure in experiments or computed by current code such as TM5-1300 (1990). In this paper, the reflected pressure is chose by TM5 empirical equation as a function of the scaled distance.

As shown in Fig. 7(a), the virtual rotation at the ends is θ , and the external virtual work done by the uniform load \bar{P} is

$$W_e = 4\theta \int_0^{L/2} \int_0^{L/2} \bar{P}(\frac{L}{2} - x) dx dy = 4\theta \bar{P} \int_0^{L/2} \int_0^{L/2} (\frac{L}{2} - x) dx dy \tag{15}$$

$$= 4\theta \bar{P} \frac{L}{2} (\frac{L^2}{4} - \frac{1}{2} \frac{L^2}{4}) = 4\theta \bar{P} \frac{L^3}{16}$$

On the other hand, as shown in Fig. 7(b), the virtual work W_p done by the blast pressure wave is computed by plus all of the virtual work done by the blast load on front face of the slab. The virtual work done by the blast pressure wave $P(x, y)$ is

$$W_p = 4\theta \int_0^{L/2} \int_0^{L/2} P(x, y)(\frac{L}{2} - x) dx dy$$

$$= 4\theta \int_0^{L/2} \int_0^{L/2} [P_{s1} + \frac{2}{L}(P_{s2} - P_{s1})(x + y) + \frac{4}{L^2}xy(P_{s3} + P_{s1} - 2P_{s2})](\frac{L}{2} - x) dx dy \tag{16}$$

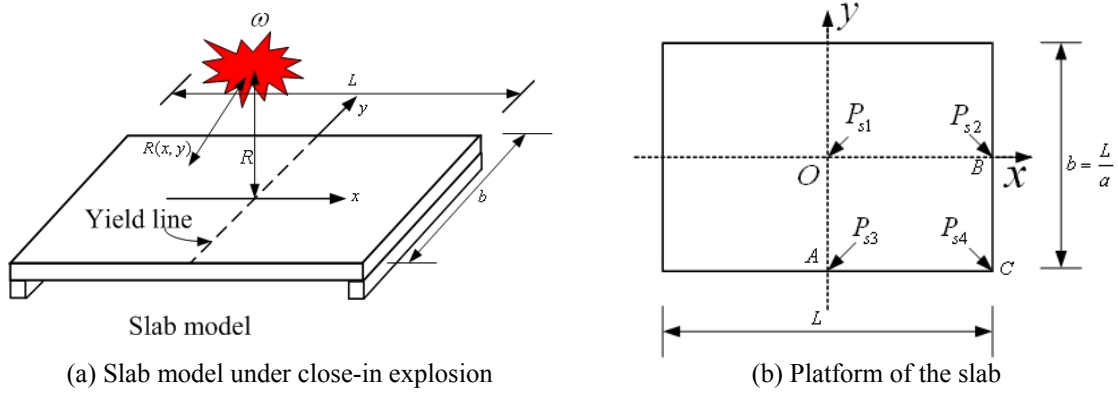
$$= 4\theta [-P_{s1} \frac{L^3}{32} + P_{s2} \frac{13L^3}{96} - P_{s3} \frac{L^3}{24}]$$

Using the principle of virtual work and equating Eqs. (15) and (16), the uniform peak blast pressure, \bar{P} , is given by

$$W_e = 4\theta \bar{P} \frac{L^3}{16} = 4\theta [-P_{s1} \frac{L^3}{32} + P_{s2} \frac{13L^3}{96} - P_{s3} \frac{L^3}{24}] = W_p \tag{17}$$

$$\bar{P} = -P_{s1} \frac{L^3}{2} + P_{s2} \frac{13L^3}{6} - P_{s3} \frac{2L^3}{3} \tag{18}$$

For a rectangle reinforced concrete slab with different ratio a of the span length L to its slab width b , the same producer is used to compute the equivalent uniform blast load. The slab is



(a) Slab model under close-in explosion (b) Platform of the slab

Fig. 8 Failure mechanism of a simply supported rectangle reinforced concrete slab

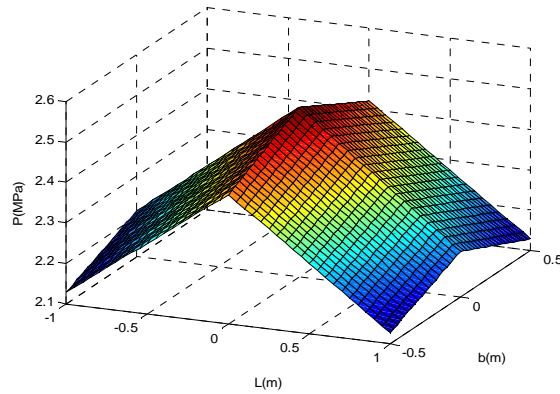


Fig. 9 A typical three-dimensional peak pressure distribution of the rectangle RC slab

shown in Fig. 8. The peak pressure of the edge B is noted as P_{s2} , the peak pressure of the edge A is noted as P_{s3} , and the peak pressure of the corner C is noted as P_{s4} which is shown in Fig. 8(b).

The peak pressure function $P(x, y)$ can be simply expressed as Es. (19). A typical peak pressure $P(x, y)$ distribution on a rectangle slab is shown in Fig. 9.

$$P(x, y) = P_{s1} + \frac{2}{L}(P_{s2} - P_{s1})x + \frac{2a}{L}(P_{s3} - P_{s1})y + \frac{4a}{L^2}xy(P_{s4} - P_{s2} - P_{s3} + P_{s1}), \tag{19}$$

$$0 \leq x \leq L/2, \quad 0 \leq y \leq L/(2a)$$

The external virtual work done by the uniform load \bar{P} is

$$W_e = 4\theta \int_0^{L/2} \int_0^{L/(2a)} \bar{P}(\frac{L}{2} - x) dx dy = 4\theta \bar{P} \int_0^{L/2} \int_0^{L/(2a)} (\frac{L}{2} - x) dx dy \tag{20}$$

$$= 4\theta \bar{P} (\frac{L}{2} \frac{L^2}{4a} - \frac{1}{2} \frac{L^2}{4} \frac{L}{2a}) = 4\theta \bar{P} \frac{L^3}{16a}$$

And the virtual work done by the blast pressure wave $P(x, y)$ is

$$W_p = 4\theta \int_0^{L/2} \int_0^{L/(2a)} P(x, y) \left(\frac{L}{2} - x\right) dx dy = 4\theta \frac{L^3}{a} \left[-P_{s1} \frac{1}{32} + P_{s2} \frac{1}{16} + P_{s3} \frac{7}{96} - P_{s4} \frac{1}{24}\right] \quad (21)$$

Then \bar{P} , is given by

$$W_e = 4\theta \bar{P} \frac{L^3}{16a} = 4\theta \frac{L^3}{a} \left[-P_{s1} \frac{1}{32} + P_{s2} \frac{1}{16} + P_{s3} \frac{7}{96} - P_{s4} \frac{1}{24}\right] = W_p \quad (22)$$

$$\bar{P} = \left[-P_{s1} \frac{1}{2} + P_{s2} + P_{s3} \frac{7}{6} - P_{s4} \frac{2}{3}\right] \quad (23)$$

It is found from Eq. (23) that the peak equivalent uniform blast pressure has no relationship with the span length to its slab width ratio a , and only influence by peak pressures of the four characteristic points in Fig. 8.

In this paper, the blast load loaded on the slab of different points such P_{s1} and P_{s4} is on the assumption of the same arrival time and calculated the same time as shown before. After the peak pressure of the equivalent blast pressure is got by above producer, the center blast load impulse is chose as the equivalent blast load impulse (TM5-1300 1990, UFC-3-340-02 2008). In this paper, the equivalent blast pressure is simplified to be triangular loading as shown in TM5-1300 (TM5-1300 1990, UFC-3-340-02 2008), and the load duration t_d can be computed as

$$t_d = \frac{2I_{s1}}{\bar{P}} \quad (24)$$

where I_{s1} is the center blast load impulse, and \bar{P} is the peak equivalent uniform blast pressure computed by Eqs. (18) and (23) for square and rectangle reinforced concrete slabs respectively.

The equivalent uniform blast load is derived based on the assumption of flexural failure in center yield line, thus, it must be used with caution for scaled distance less than 0.4 and other damage mode such as spalling and perforation of the slab.

4. Validation using experimental data

To test the utility of the equivalent blast pressure method of SDOF model, the predictions were compared with maximum displacement data from blast testing results on one-way fixed supported 1m wide square RC slabs done by the authors (Wang *et al.* 2012b) and one-way fixed supported 2m long rectangle slabs by Wu (2009). The failure mode is the same with simple fixed slabs on the assumption that the slabs will be fail in the center line in flexure.

4.1 One-way square slabs

Dimensions of the square slabs are given in Fig. 10. These specimens were constructed with a 6mm

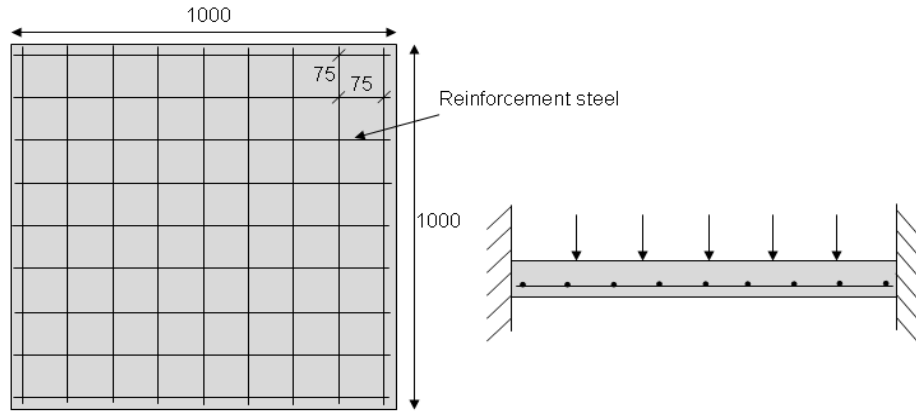


Fig. 10 Geometry of the square RC slab (in mm)



Fig. 11 Test device

diameter bar meshing that was spaced in distance of 75 mm from each other in the major bending plane ($\rho = 1.43\%$) and in distance of 75 mm from each other in the other plane ($\rho = 1.43\%$), where ρ is reinforcement ratio. The thickness of the concrete cover was 20 mm. The concrete had a cylinder compressive strength of 39.5 MPa, tensile strength of 4.2 MPa and Young's modulus of 28.3 GPa. The reinforcement is of yield strength of 600 MPa and Young's modulus of 200 GPa.

A steel frame was built on the ground (Fig. 11) to ensure that the specimens are firmly placed. The steel members used for the frame consisted of 8 mm thick steel angles. The RC slab was clamped down on each side of the steel angle to prevent uplifting during the tests. Wooden bars of the same width and length as the steel angle were placed on two sides, between the specimen and the frame, to provide uniform supporting conditions and prevent direct impact damage on the specimen edges. The specimens were estimated using the fixed supports, although the end restraint in the test was somewhere between fixed and pinned, and the extent of fixity likely depends on the magnitude of the imposed blast load and the damage sustained by the restraints.

TNT explosive is used in explosion tests because it is a standard high explosive and very safe chemically, easier to cast. A detonator is inserted on the top of TNT. The mass of TNT is set at 0.2 kg

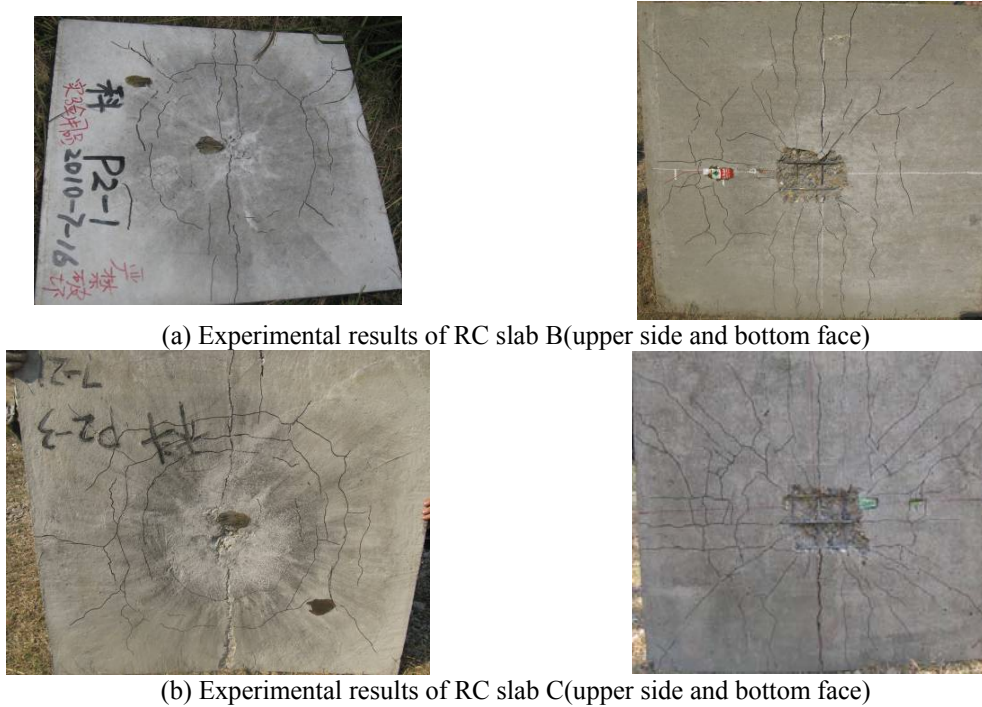


Fig. 12 Typical Experimental results of RC slabs

Table 2 Experimental program of square slabs

Blast test	Slab name	Explosive mass (kg)	Scale distance(m/kg ^{1/3})	Damage level
I	A	0.2	0.684	Low damage
II	B	0.31	0.591	Moderate damage
III	C	0.46	0.518	Moderate damage
IV	D	0.55	0.488	High damage

to 0.53 kg to examine the effect of mass of explosive on the damage of concrete slabs. As shown in Fig. 11, the charge was suspended above the test as specimens to a specific stand-off distance by a rope. Table 2 summarizes the test program. The standoff distances were measured from the underside of the explosive to the top surface of the slab. In the experiments, the standoff distance is chosen to be 400mm. Typical test results are shown in Fig. 12. More experiment detail results of the slabs can be seen in Wang *et al.* (2012b).

The flowchart of the proposed procedure to generate the resistance function and solving the equation of motion for the required dynamic response is shown in Fig. 13. The approach consists of two coordinate steps for evaluating the flexural response: compute the equivalent uniform blast load parameters and generate flexural resistance function. For the flexural mode or response, the resistance has to be re-calculated at each time step since the resistance is dependent on the center displacement for the slab.

The comparisons of experiments and equivalent SDOF results are shown in Table 3. The equivalent uniform peak pressure and load duration which are computed by Eqs. (18) and (24) are also listed in the table. The peak pressures of the four characteristic points and impulse are

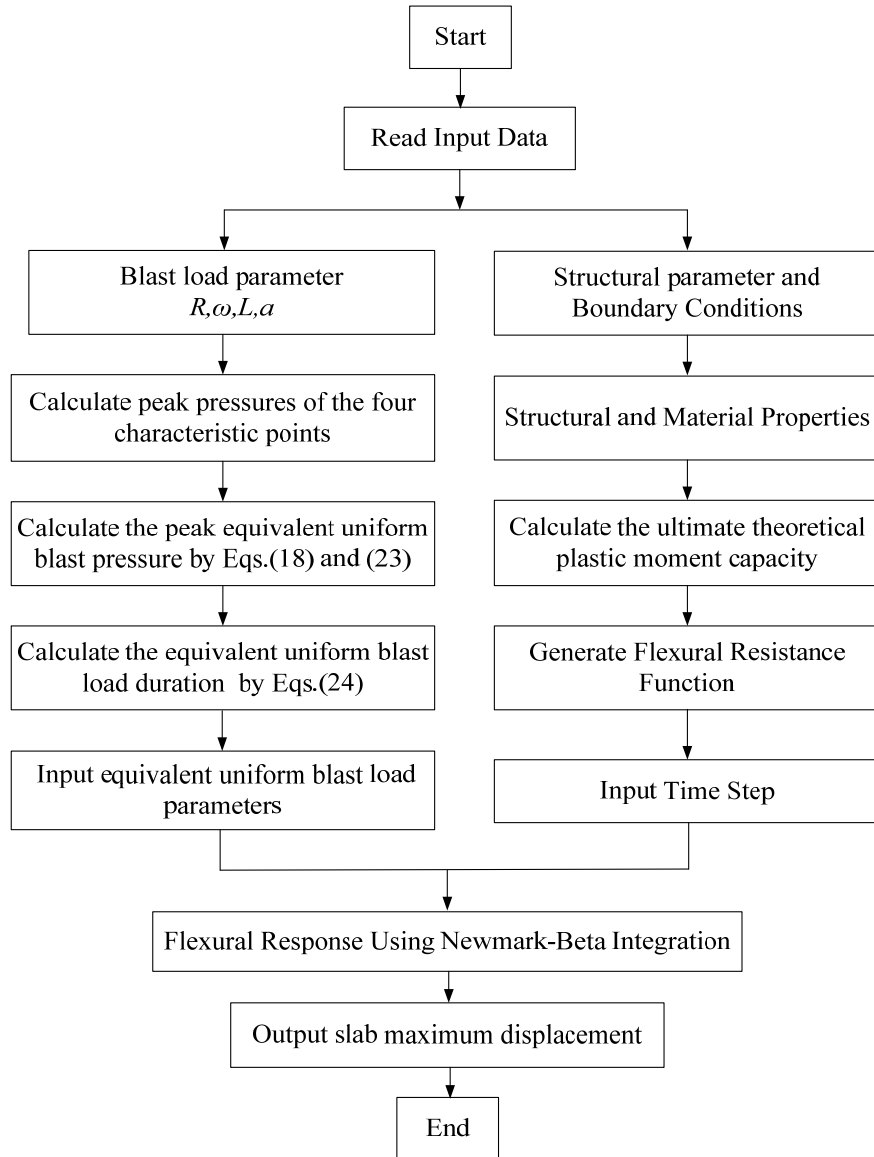


Fig. 13 Flow chart to compute the structure response

computed by current code such as TM5 (1990). It is found that with the increasing of TNT charge weight, the equivalent uniform peak pressures increase and load duration decrease a little more. The equivalent SDOF results accurately predicted maximum displacement responses in first three tests. Blast test IV all failed with high damage in both experiment and equivalent SDOF result. Although slab B and C clearly show localized damage associated with crater formation, spalling, and scabbing, effects, these are stress wave and material damage mechanisms that cannot be included in a structural response calculation. However, due to the limitation of the SDOF system shown in (PDC-TR-06-01(Rev1) 2008), the damage of the slab such as breach, fragment penetration, rebar pullout, etc. often cannot be modeled directly except in the most complex finite

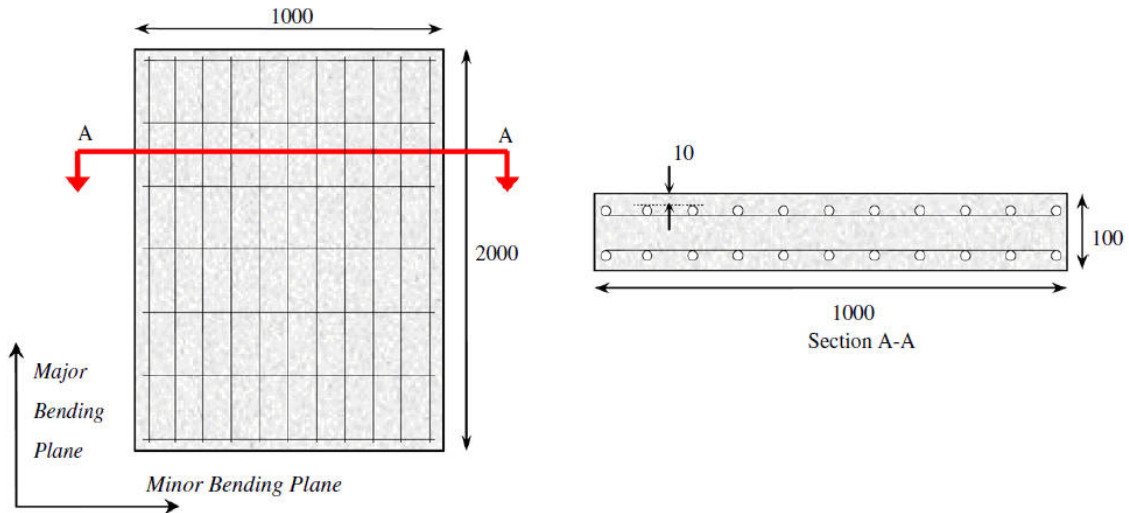


Fig. 14 Geometry of the rectangle RC slab (in mm)

Table 3 Comparison of maximum deflections from predictions and tests of square slabs

Blast test	Experiment results		Equivalent SDOF results		Prediction error (%) for deflection
	Max central deflection (mm)	Equivalent uniform peak pressure (MPa)	Load duration (ms)	Max Central deflection (mm)	
I	10	1.264	1.25	9.7	-3
II	15	3.015	0.83	17.4	16
III	35	5.503	0.63	37.8	8
IV	/	6.821	0.59	51.7	/

element analyses and the biggest center displacement of the slab would be affected very little by such localized damage.

4.2 One-way rectangle slabs

Details of the rectangle slab and other test data can be found in Wu *et al.* (2009). Dimensions of the slab are given in Fig. 14. These specimens were constructed with a 12 mm diameter mesh that was spaced in distance of 100 mm from each other in the major bending plane ($\rho = 1.34\%$) and in distance of 200 mm from each other in the minor plane ($\rho = 0.74\%$) where ρ is reinforcement ratio. The thickness of the concrete cover was 10 mm. The concrete had a cylinder compressive strength of 39.5 MPa, tensile strength of 8.2 MPa and Young's modulus of 28.3 GPa. The reinforcement was of yield strength 600 MPa and Young's modulus 200 GPa. The experimental test program is summarized in Table 4. The explosive charge was suspended above the center of the slab as described in Wu *et al.* (2009).

More experiment detail results of the rectangle slabs can be seen in Wu *et al.* (2009). The flowchart of the proposed procedure to generate the resistance function and solving the equation of motion for the required dynamic response is also shown in Fig. 13. The comparisons of

Table 4 Experimental air blast program of rectangle slabs

Blast	Slab name	Dimension (mm)	Reinforcement ratio(%)	Stand-off distance(m)	Scaled distance(m/kg ^{1/3})	Explosive mass(g)
NRC-1	E	2000x1000x100	1.34	3	3.0	1007
NRC-2	E	2000x1000x100	1.34	3	1.5	8139
NRC-3	F	2000x1000x100	1.34	1.4	0.93	3440
NRC-4	E	2000x1000x100	1.34	1.5	0.75	8213

Table 5 Max deflection compared with experiments of rectangle slabs

Blast test	Experiment results		Equivalent SDOF results		Prediction error (%) for deflection
	Max central deflection (mm)	Equivalent uniform peak pressure (MPa)	Load duration (ms)	Max Central deflection (mm)	
NRC-1	1.8	0.311	1.44	2.02	12
NRC-2	10.5	2.358	0.88	10.51	0.1
NRC-3	13.9	7.388	0.35	15.09	8.5
NRC-4	38.9	13.455	0.32	37.69	-3.1

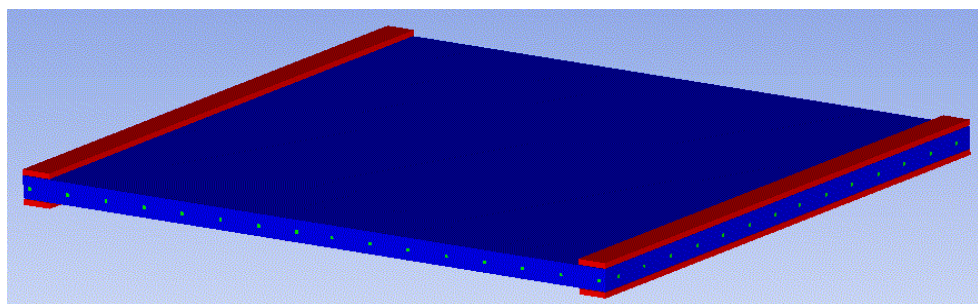


Fig. 15 Finite element model of the specimen

experiments and equivalent SDOF results of the rectangle slab are shown in Table 5. The equivalent uniform peak pressure and load duration are also listed in the table. One can find that based on Eqs. (23) and (24), the equivalent uniform peak pressures also increase and load duration decrease a little more with reducing of the scaled distance. The equivalent SDOF results accurately predicted maximum displacement responses in all tests.

5. Comparison of different analysis methods

To illustrate issues associated with analysis of structural components subjected to blast loads, the displacement response of specimens A, B, and C of Table 2 were estimated by conventional SDOF, finite element and the new equivalent SDOF.

The conventional SDOF analysis was performed using the industry-standard approach first proposed by Biggs (1964) as described in Section 2. The center pressure load history is chosen as the uniform blast load history. The computer code AUTODYN (2006) with solid element model was used to perform the finite element analysis. A three-dimensional solid model including

Table 6 Predictions of maximum deflections

Blast test	Max central deflection (mm)			Prediction error (%) for deflection			
	Experiment results	Conventional SDOF	New equivalent SDOF	AUTODYN	Conventional SDOF	New equivalent SDOF	AUTODYN
I	10	111	9.7	9.2	1000	-3	-8
II	15	223	17.4	13.7	1387	16	-8.7
III	35	415	37.8	32.6	1085	8	-6.8

explosive, air and RC slab with concrete and reinforcing bars being separated is created to simulate the experiments, and the sophisticated concrete and reinforcing bar material models taking into account the strain rate effects and the appropriate coupling at the air-solid interface are applied to simulate the dynamic response of RC slab. In this study, RHT dynamic damage model (Riedel *et al.* 1999) for concrete is adopted. The reinforcement steel is modeled by the Johnson and Cook material model (Johnson and Cook 1983). Air is modeled by an ideal gas EOS and high explosives (TNT) are typically modeled by using the Jones-Wilkins-Lee (JWL) EOS. All the material parameters from the AUTODYN material library (AUTODYN 2006) are used. The specimen was modeled using solid brick elements as shown in Fig. 15. The element size is 3mm, the element number for the RC slab is 397293, and it is 450000 for the air and the explosive in the simulations.

The predicted maximum deflections of the tests using the conventional SDOF, finite element and new equivalent SDOF model are summarized in Table 6. The finite element and new equivalent SDOF model predictions of the maximum deflection are much closer to the measured maximum deflections than the conventional SDOF predictions. The use of the conventional SDOF model gave a very conservative prediction (the smallest error is 1387%), in part because center pressure load history was used in the calculation of the conventional equivalent SDOF load. Although the AUTODYN model also predicted the maximum deflection well, much time was required to prepare the FE model and reduce the data.

6. Conclusions

Since it can be very difficult to model component response to blast loads with complex spatial load distributions using a conventional SDOF analysis because the load factor in SDOF analyses almost always assumes spatially uniform loading, a new effective model for calculation of the equivalent uniform blast load for non-uniform blast load such as close-in explosion of a one-way square and rectangle reinforced concrete slab is proposed in this paper. A theoretical formula for peak equivalent uniform blast load is proposed with respect of peak pressures of the four characteristic points of the slab.

Based on the new effective model of blast pressure and equivalent SDOF method, the response of the slab is computed for different RC slabs under non-uniform blast load. A comparison between the measured and analytical responses was made and the largest difference was only 16%, indicating that the new equivalent SDOF model can accurately predict the response of a square and rectangle RC slabs to blast loads. The results are also compared with those obtained by conventional SDOF analysis and finite element (FE) analysis using solid elements. It is shown that the new model is more accurate than the conventional SDOF analysis and is running faster than

the finite element (FE) analysis.

However, unlike the finite element analysis that divides a member into three dimensional solid elements, the new equivalent SDOF model based on the conventional SDOF method with one key point of the slab such as center of the slab. Far fewer elements are used in the new equivalent SDOF model than elements in the finite element model, leading to a substantial reduction in the computational effort. Conventional SDOF analysis is straightforward and suitable for use in a design office but the results are based on the center blast pressure history of the slab and it can be substantially conservative with much higher of the results. The new equivalent SDOF model can capture many of the important features of a finite element analysis, provides accurate results, is computationally efficient and is ideally suited for slab design and blast assessment.

It should be noted that this approach is valid only for slab deformed mechanism follow the assumed displaced shape. The method of calculation of the equivalent uniform blast load on slabs with other displaced shape such as two-way supported slabs should be investigated in the future research.

Acknowledgements

This work is supported by the National Natural Science Foundation of China (No.11202236), and the Scientific Foundation of National University of Defense Technology (No. JC11-02-18). The financial supports are gratefully acknowledged. We thank two referees for their detailed comments that have helped improve this paper substantially.

Reference

- AUTODYN (2006), "Theory Manual. Century Dynamics".
- Bangash, M.Y. H. and Bangash, T. (2006), *Explosion-resistant buildings design, analysis, and case studies*, Springer, Berlin.
- Biggs, J.M. (1964), *Introduction to Structural Dynamics*, McGraw-Hill.
- Islama, A.K.M.A. and Yazdani, N. (2008), "Performance of AASHTO girder bridges under blast loading", *Eng. Struct.*, **30**, 1922-1937.
- Johnson, G.R. and Cook, W.H. (1983), "A constitutive model and data for metals subjected to large strains, high strain rates and high temperatures", *Proceedings of the seventh international symposium on ballistics*, The Hague, The Netherlands.
- Jones, J., Wu, C., and Oehlers, D.J. *et al.* (2009), "Finite difference analysis of simply supported RC slabs for blast loadings", *Eng. Struct.*, **31**, 2825-2832.
- Krauthammer, T. (1999), "Blast-resistant structural concrete and steel connections", *Int. J. Impact Eng.*, **22**(9-10), 887-910.
- Krauthammer, T. (2008), *Modern Protective Structures*, CRC Press.
- LS-DYNA (2007), *Version 971 Manual*, Livermore Software Technology Corporation (LSTC), Livermore (CA, USA).
- Luccioni, B.M., Ambrosini, R.D. and Danesi, R.F. (2004), "Analysis of building collapse under blast loads", *Eng. Struct.*, **26**(1), 63-71.
- Mays, G.C. and Smith, P.D. (1995), *Blast effects on buildings-design of buildings to optimize resistance to blast loading*, Thomas Telford, London.
- Nash, P.T., Vallabhan, C.V.G. and Knight, T.C. (1995), "Spall damage to concrete walls from closein cased

- and uncased explosions in air”, *ACI Struct. J.*, **92**(6), 680-688.
- Newmark, N.M. (1962), “A method of computation for structural dynamics”, *American Society of Civil Engineers Transactions*, Paper No. 3384, **127**.
- Ohkubo, K., Beppu, M. and Ohno, T. *et al.* (2008), “Experimental study on the effectiveness of fiber sheet reinforcement on the explosive-resistant performance of concrete plates”, *Int. J. Impact Eng.*, **35**(12), 1702-1708.
- Osteraas, J.D. (2006), “Murrah building bombing revisited: a qualitative assessment of blast damage and collapse patterns”, *J. Perform. Constr. Facil.*, **20**(4), 330-335.
- PDC-TR-06-01(Rev1) (2008), Methodology Manual for the Single-Degree-of-Freedom Blast Effects Design Spreadsheets (SBEDS), US Army Corps of Engineers.
- Rabczuk, T. and Eibl, J. (2003), “Simulation of high velocity concrete fragmentation using SPH/MLSPH”, *Int. J. Numer. Meth. Eng.*, **56**(10), 1421-1444.
- Rabczuk, T., Eibl, J. and Stempniewski, L. (2004), “Numerical analysis of high speed concrete fragmentation using a meshfree Lagrangian method”, *Eng. Fract. Mech.*, **71**(4-6), 547-556.
- Riedel, W., Thoma, K. and Hiermaier, S. (1999), “Numerical analysis using a new macroscopic concrete model for hydrocodes”, *Proceedings of 9th international symposium on interaction of the effects of munitions with structures*, 315-322.
- Silva, P.F. and Lu, B. (2007), “Improving the blast resistance capacity of RC slabs with innovative composite materials”, *Composites: Part B*, **38**, 523-534.
- Silva, P.F. and Lu, B. (2009), “Blast resistance capacity of reinforced concrete slabs”, *J. Struct. Eng.*, **135**(6), 708-716.
- Tedesco, J.W., McDougal, W.G. and Ross, C.A. (1999), *Structural Dynamics: Theory and Applications*, Addison-Wesley Longman Inc, Menlo Park, CA.
- TM5-1300 (1990), Structures to resist the effects of accidental explosions, US Department of the Army, Navy and Air Force Technical Manual.
- UFC-3-340-02 (2008), Unified facilities criteria UFC DOD structures to resist the effects of accidental explosions, US Department of Defense.
- Wang, W., Zhang, D. and Lu, F.Y. (2012a), “The influence of load pulse shape on pressure-impulse diagrams of one-way RC slabs”, *Struct. Eng. Mech.*, **42**(3), 363-381.
- Wang, W., Zhang, D. and Lu, F.Y. *et al.* (2013a), “Pressure-impulse diagram with multiple failure modes of one-way reinforced concrete slab under blast loading using SDOF method”, *Journal of Central South University*, **20**(2), 510-519.
- Wang, W., Zhang, D. and Lu, F.Y. *et al.* (2012b), “Experimental study on scaling the explosion resistance of a one-way square reinforced concrete slab under a close-in blast loading”, *Int. J. Impact Eng.*, **49**, 158-164.
- Wang, W., Zhang, D. and Lu, F.Y. *et al.* (2013b), “Experimental study and numerical simulation of the damage mode of a square reinforced concrete slab under close-in explosion”, *Eng. Failure Anal.*, **27**, 41-51.
- Wu, C., Oehlers, D.J. and Rebstrost, M. *et al.* (2009), “Blast testing of ultra-high performance fibre and FRP-retrofitted concrete slabs”, *Eng. Struct.*, **31**, 2060-2069.
- Xu, K. and Lu, Y. (2006), “Numerical simulation study of spallation in reinforced concrete plates subjected to blast loading”, *Comput. Struct.*, **84**, 431-438.
- Zhou, X.Q., Hao, H. and Deeks, A.J. (2005), “Modeling dynamic damage of concrete slab under blast loading”, *Proceeding of the 6th Asia-Pacific Conference on Shock and Impact Loads on Structures*, Perth, WA, Australia .